Evaluation of size effect on strain-controlled fatigue behavior of a quench and tempered rotor steel: Experimental and numerical study

Shun-Peng Zhu[a,b,*], Stefano Foletti[b], Stefano Beretta[b]

[a] School of Mechanical and Electrical Engineering, University of Electronic Science and Technology of China, Chengdu 611731, China
[b] Department of Mechanical Engineering, Politecnico di Milano, Via La Masa 1, 20156 Milan, Italy

Combining the weakest-link theory with fatigue crack growth modeling, this study presents a mechanical-probabilistic modeling of specimen size effect for 30NiCrMoV12 steel in a low cycle fatigue (LCF) regime. Particularly, the influence of specimen size on fatigue life is quantified by experiments in strain-controlled fatigue and crack propagation. Experimental results from replica tests with three geometrical specimens indicate that nearly all of its fatigue life consists of multiple surface cracking with mutual interactions and coalescences. A probabilistic procedure for multiple surface fracture simulation is then established by incorporating random processes of crack formation, propagation and coalescence between dispersed surface cracks. Moreover, an evaluation of surface damage evolution is elaborated based on statistical physics for different structural sizes/volumes, which showed good agreement between analytical life distributions and test results.

Keywords:
Fatigue
Size effect
Weakest-link theory
Crack coalescence
Life prediction

1. Introduction

Fatigue and fracture tests are normally conducted on small test specimens of structural materials used for aircraft engines, nuclear power plants, and high-speed trains. More specifically, to satisfy safety demands, accurate assessment of fatigue life is required in structural integrity design and assessment. However, due to various factors, in-cluding specimen size, heat treatment, microstructure, and load con-ditions (temperature and frequency), a comprehensive understanding of fatigue and fracture behavior has not yet been attained [1]. In practice engineering, combinations of these factors usually contribute to a significant scatter in the fatigue life data or performance, which is one of the most critical factors for designing structure [2–4]. For the 30NiCrMoV12 as-quenched and tempered steel of research interest, which was developed for aerospace application and then adopted as high performance solution for railway axles due to its excellent me-chanical properties, its heat treatment process has been optimized for the required strength and toughness through appropriate micro-structure (martensite packets, blocks and laths) and carbide pre-cipitates. Specifically, Zheng et al. [5] investigated the influence of austenitizing temperature and martensitic microstructure on carbide precipitates and mechanical properties during tempering in as-quen-ched and tempered 30NiCrMoV12 alloy steel. In addition, quantification of the size effect, i.e. how to extrapolate from test specimens to real components with different volumes, is critically important for ensuring structural integrity when designing structural/mechanical components.

In predicting the fatigue life of full scale components or structures, such as engine hot section components and high-speed train railway axles [6,7], the specimen size effect is critical when utilizing the laboratory testing of small standard specimens as the reference basis. In other words, fatigue testing on large specimens for those structures is not always possible due to financial/technical considerations (availability of testing equipment, test costs and time). Therefore, characterizing the influence of specimen size on fatigue life is needed and corresponding methods are lacking, especially a robust probabilistic method for quantifying the specimen size effect.

Until now, most conventional methods treated the effect of specimen size on fatigue life as a negative one, namely this effect reduces fatigue strength/life for an increase of specimen size [8–11]. From the viewpoint of defect-induced fatigue, the size of the most dangerous defect generally increases with the size/scale of engineering structure/component [12]. However, few guidelines, recommendations or mandatory regulations have launched well on the strength assessment of structures with different sizes/volumes under different loadings. Among them, the treatment of size effect by the German FKM guideline is purely empirical, which is determined from empirical design curves/formulas [10,13,14]. The application of the specimen size effect to other cross-sectional shapes/volumes and stress distribution conditions

* Corresponding author at: School of Mechanical and Electrical Engineering, University of Electronic Science and Technology of China, Chengdu 611731, China.
E-mail address: zspeng2007@uestc.edu.cn (S.-P. Zhu).

Published Journal Article available at: https://doi.org/10.1016/j.msea.2018.08.073

Nomenclature

a	Crack length
b	Fatigue strength exponent
d	Crack tip distance
α	Weibull scale parameter
n	Number of loading cycles
β	Weibull shape parameter
n'	Cyclic strain hardening exponent
D_0	Diameter of cross section
$\Delta\sigma_{eff}$	Effective stress range
$\Delta\varepsilon_{p,eff}$	Effective plastic strain range
K'	Cyclic strength coefficient
λ	Crack density
ε_a	Strain amplitude
N_f	Number of cycles to failure
$\gamma_{standard}$	Scale factor for standard specimen from the reference small specimen
a_i, a_f	Initial and final crack length
c	Fatigue ductility exponent
E	Elastic modulus
σ_y	Yield strength
R	Stress ratio
P_f	Failure probability
σ_f'	Fatigue strength coefficient
ε_f'	Fatigue ductility coefficient
L_0	Gauge length
v	Poisson's ratio
ΔJ_{eff}	Effective cyclic J-integral
$\Delta\varepsilon_t$,$\Delta\varepsilon_e$, ε_p	Total, elastic and plastic strain range
$\Delta\sigma$	Stress range
r_p	Diameter of plastic deformation zone
γ_{large}	Scale factor for large specimen from the reference small specimen

is often not explained as well as the robustness of the low cycle fatigue (LCF) resistance against specimen size [15]. One of the commonly-used way to characterize the size effect by means of the weakest-link theory and the statistics of extremes. Recently, by combining the theory of critical distance with the volumetric approaches, Wang et al. [16] explored statistical size effect of TA19 titanium alloy for different scales of test sections with central circular holes, and pointed out that both the geometrical and statistical size effect should be taken into account for analyzing the combined effect of size and notch in practice. By interpreting the Coffin-Manson parameters as geometry-independent parameters, Schmitz et al. [17] developed a probabilistic fatigue model to consider the effects of specimen size and inhomogeneous strain fields of polycrystalline metals. Later, they [18,19] calibrated the geometry-independent model parameters from the hazard density approach and the surface integration over the FEA stress, then elaborated a probabilistic procedure to predict the fatigue crack initiation life distribution of arbitrarily shaped parts by considering the combined size and notch support effect. Blasón et al. [20] investigated the transferability of fatigue properties of 42CrMoS4 steel alloy with different sizes, and quantified the twofold scale effects for the statistical interpretation of cracking behavior. However, a probabilistic interpretation between the propagation crack growth rate and the fatigue failure lifetime is lacking. Therefore, to explain the specimen size effect toward in-creasing reliability of fatigue critical components, metallurgical and mechanical details must be considered in fatigue modeling and life assessment.

Note from [21,22] that fatigue life of ductile steels is generally dominated by crack propagation life rather than crack initiation life, which also agrees well with the experimental observations of current study (see Section 2). Namely, the influence of specimen size on the fatigue crack propagation rate, particularly on the scatter in small fatigue crack growth, has been viewed as the main factor influencing the fatigue life. Specifically, the influence of specimen size on mechanical properties varies from the type and local features of the component/structure, while the effect of inclusion can be neglected [21]. The challenge will be to use not only the governing factors, such as local microstructure, local stress/strain, surface conditions and damage physics, but also statistical approaches to understand the size effect in a LCF regime. Among them, surface microcracks, which describe the fatigue damage from the viewpoint of random damage events, have been studied recently to fully understand the fatigue failure mechanism [23–31], which is essential for fatigue life prediction and inspection routines for the development of cracks or defects. These cracks usually initiate at the specimen surface during the initial stage of fatigue tests and then extend to failure with accelerated crack growth rates through coalescence under high crack density. For life assessment of engineering designs with different sizes, lifing procedures based on Monte Carlo simulation have shown advantages on accounting for the statistical scatter of experimental life of materials with different microstructures [29,32].

In this regard, this paper attempts to quantify the influence of specimen size on fatigue life of 30NiCrMoV12 steel from the viewpoint of mechanical-probabilistic modeling and numerical simulation of surface cracking behavior. In particular, an alternative procedure for practical fatigue design by considering size effect will be critically investigated. This paper contains the following parts. In Section 2, strain-controlled fatigue experiments are carried out on three geometries of specimens to investigate the specimen size effect. Moreover, its cyclic response and surface cracking behavior are explored. Section 3 elaborates a mechanical-probabilistic prediction of specimen size effect on total fatigue life through combining the weakest-link theory and crack propagation modeling in a LCF regime, which quantifies the specimen size effect by summing the effect of statistical defects and that of crack propagation. Combining analytical with experimental studies, Section 4 presents and validates a numerical procedure for multiple fracture evaluation by considering the effects of crack initiation, crack propagation and crack coalescence under different specimen geometries. Section 5 compares the present work with other studies and elaborates consequences for fatigue design with and/or without defects. Section 6 summarizes the theoretical and experimental results of the current work.

2. Experimental program

2.1. Material

Low cycle fatigue tests have been conducted on specimens with three different geometries of similar shape, which are designed ac-cording to ASTM standard E606 [33], E739 [34] and prepared by electro-chemical polishing [35]. Fig. 1 shows the geometry of standard specimen used in the strain-controlled fatigue tests. Three different specimen geometries have been manufactured to study statistical size effects. The diameter (D_0) and the gauge length (L_0) of the three specimens as well as the number of tested specimens are listed in Table 1. Particularly, the minimum number of specimens required in $S-N$ testing was determined according to the ASTM standard E739, in which the replication index is calculated as 86.67%. The specimens were made of 30NiCrMoV12 steel grade (according to UNI 6787 [36]). This alloyed steel grade comes from a very selected scrap that is melt in an Electric Arc Furnace (EAF) then refined in a Ladle Heating Furnace (LHF), and finally vacuum degassed and poured into ingots. Its heat treatment includes normalization at 900°C for structure levelling and grain size

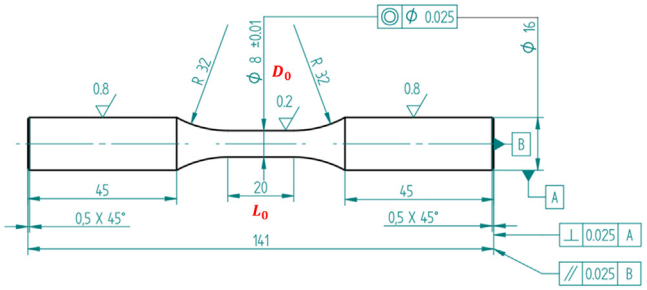

Fig. 1. Standard specimen geometry for strain-controlled fatigue tests.

Table 1
Details of the three tested specimens.

Geometry	D_0/mm	L_0/mm	Number of tested specimens
M: Standard specimen	8	20	16
S: Small specimen	3	8	28
L: Large specimen	14	36	11

refinement, then a quench treatment at 870°C and cooling in polymer (aquaquench), finally a tempering process taking at 630°C for 12 h in order to increase toughness. Chemical composition and monotonic mechanical properties of 30NiCrMoV12 are reported in Tables 2, 3, respectively.

The heat treatment temperature has significant effect on the size of the prior austenite grain (PAG): the higher is the austenitizing temperature in a range 850–1080 °C, the larger is PAG size [5]. The 30 μm grains size appears at 870 °C austenitizing temperature and it helps to increase the material strength, with a resulting good balance between strength and toughness.

2.2. Testing

In the present study, three types of strain-controlled fatigue tests were performed, including typical LCF tests and replica tests on smooth/notched specimens. Specifically, two servo-hydraulic fatigue testing machines, one with a maximum load of 100 kN was used for tension-compression testing of standard and small specimens, and an-other one with a maximum load of 250 kN for large specimens; three extensometers were used for axial displacement measurement of the three specimens. For tests with standard specimens, previous test re-sults of 30NiCrMoV12 with the same heat treatment in [37] are con-sidered together with the strain-controlled fatigue tests conducted in this analysis. All tests were conducted at strain amplitude levels be-tween 0.35% and 0.8% at load ratio $R = -1$. Fatigue lifetime of the specimen is defined according to the load drop criterion, generally 1%of the load applied in the stabilized cycle is adopted.

In this analysis, replica tests were conducted to observe the crack length for crack growth/evolution modeling on the specimen surface, particularly, some tension-compression tests were interrupted at fixed cycles and plastic replicas of the specimen surfaces were made. The crack length is measured by the projection distance of the tip-to-tip length of the crack, which is normal to the applied loading direction. The quantitative crack lengths and numbers were determined by optical microscopy. All replica tests were performed on smooth and notched standard specimens at strain amplitude $\varepsilon_a = 0.5\%$. Replicas were taken during three tests on the standard specimens, three tests on the big specimen and six interrupted tests for the small specimens.

Table 3
Mechanical properties of 30NiCrMoV12.

Elastic modulus E	197*GPa*
Yield stress σ_y	878*MPa*
Ultimate tensile strength σ_{UTS}	1045*MPa*
Elongation at fracture	21.6%
Charpy Impact energy (U notch longitudinal)	> 70 J

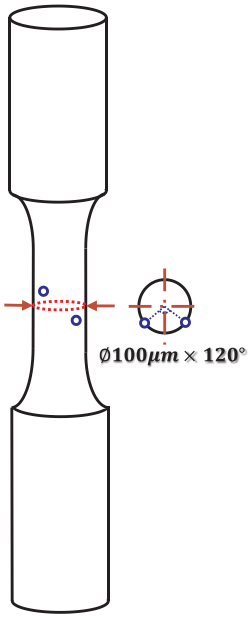

Fig. 2. Scheme of the notched standard specimen.

Moreover, two notched standard specimens were tested with replicas to evaluate its fatigue crack growth behavior. For the notched standard specimen, two micro-holes of 100 μm diameter were drilled with an angular distance of 120° and 1.5 millimeter far from the center line of the specimen (see Fig. 2). During testing, replicas of the notch are performed per 300 cycles and the crack lengths are measured. In this study, the surface cracks with length longer than 20 μm were measured including their sizes and locations to obtain the statistical distribution functions, also the crack growth behavior of specific cracks which resulted into the specimen final fracture, the surface crack den-sity variation, and the statistical crack length distribution. These data will be used as inputs for statistical simulation of multiple surface fracture (see Section 4).

2.3. Results

2.3.1. Cyclic response under strain-controlled fatigue

During LCF analysis, a so-called strain-life approach, like the Coffin-Manson equation, is often utilized for describing the relationship be-tween strain and fatigue failure lifetime under uniaxial loadings, which relates the local elastic-plastic behavior of the material,

$$\frac{\Delta\varepsilon_t}{2} = \frac{\Delta\varepsilon_e}{2} + \frac{\Delta\varepsilon_p}{2} = \frac{\sigma'_f}{E}(2N_f)^b + \varepsilon'_f(2N_f)^c \quad (1)$$

where $\Delta\varepsilon_t$, $\Delta\varepsilon_e$ and $\Delta\varepsilon_p$ are the total strain range, elastic strain range

Table 2
Chemical composition of 30NiCrMoV12.

Element	C	S	P	Mn	Cr	Ni	Cu	Si	V	Al	Sn	Ti	Mo
Weight (%)	0.280	0.006	0.004	0.580	0.790	3.060	0.130	0.340	0.090	0.035	0.008	0.006	0.510

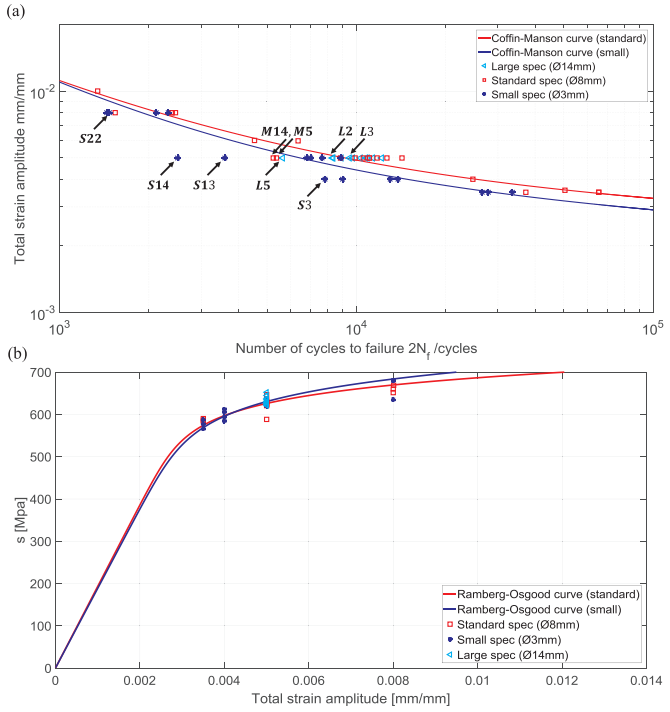

Fig. 3. Strain-controlled fatigue tests of three different specimens of 30NiCrMoV12.

Table 4
Cyclic parameters for standard and small specimens.

	σ_f'/MPa	b	ε_f'	c	n'	K'/MPa
M	1052.4	− 0.0534	0.8252	− 0.6825	0.0783	1068.3
S	1212.6	− 0.0749	1.6042	− 0.7833	0.0956	1159

and plastic strain range, respectively; N_f is the number of cycles to failure under cyclic loadings; σ_f' and b are the fatigue strength coefficient and exponent, respectively; ε_f' and c are the fatigue ductility coefficient and exponent.

Through fitting the elastic and the plastic parts of Eq. (1) from fatigue life separately, the four coefficients $\{\sigma_f', \varepsilon_f', b, c\}$ of Coffin-Manson equation can be obtained for each specimen size. When using Eq. (1) for fatigue analysis, the Ramberg-Osgood equation described the stress-strain behavior of the material by

$$\frac{\Delta\varepsilon_t}{2} = \frac{\Delta\varepsilon_e}{2} + \frac{\Delta\varepsilon_p}{2} = \frac{\Delta\sigma}{2E} + \left(\frac{\Delta\sigma}{2K'}\right)^{\frac{1}{n'}} \tag{2}$$

where $\Delta\sigma$ is the applied stress range; K' and n' are the cyclic strength coefficient and the cyclic strain hardening exponent, respectively.

Through correlating both of the elastic and plastic parts in Eqs. (1) and (2), the dependence of the six parameters can be expressed as

$$\begin{cases} \sigma_f' = K'(\varepsilon_f')^{n'} \\ n' = \frac{b}{c} \end{cases} \tag{3}$$

Using Eq. (1) to Eq. (3), cyclic response and fatigue behavior of the three specimen sizes can be plotted as shown in Fig. 3, and cyclic parameters of both Coffin-Manson and Ramberg-Osgood curves are fitted as listed in Table 4. Moreover, fracture surfaces of all failed specimens have been examined by a scanning electron microscope (SEM), note that multiple cracks initiated on the specimen surface and propagated with mutual interactions and coalescences. Particularly, several specimens with much shorter lives marked in Fig. 3**(a)** are due to the strong interactions and coalescences of multiple surface cracks,

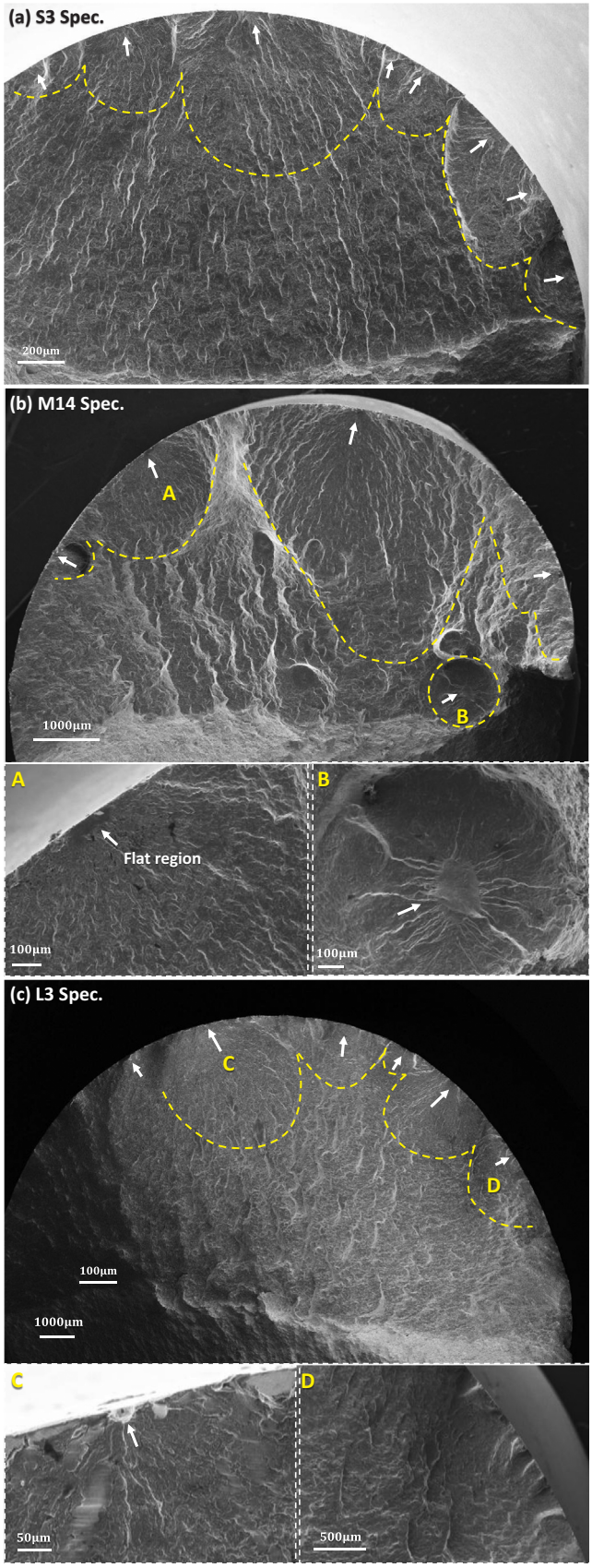

Fig. 4. Multiple surface cracks of (a) small, (b) standard and (c) large specimen.

Table 5
Experimental mean and scatter of lifecycles of three geometrical specimens.

N_f~$LN(\mu,\sigma^2)$	ε_a = 0.35%	ε_a = 0.4%	ε_a = 0.5%	ε_a = 0.8%
Small spec.	(4.1640,0.0541^2)	(3.7245,0.1204^2)	(3.4434,0.2164^2)	(2.9829,0.1101^2)
Standard spec.	(4.4336,0.1417^2)	–	(3.6806,0.1557^2)	(3.0142,0.1111^2)
Large spec.	–	–	(3.6742,0.0914^2)	–

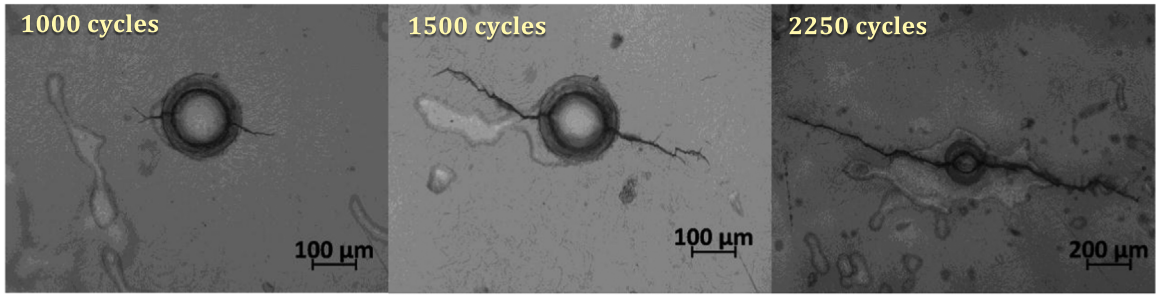

Fig. 5. Crack growth measurement near the micro-hole of M1.R specimen.

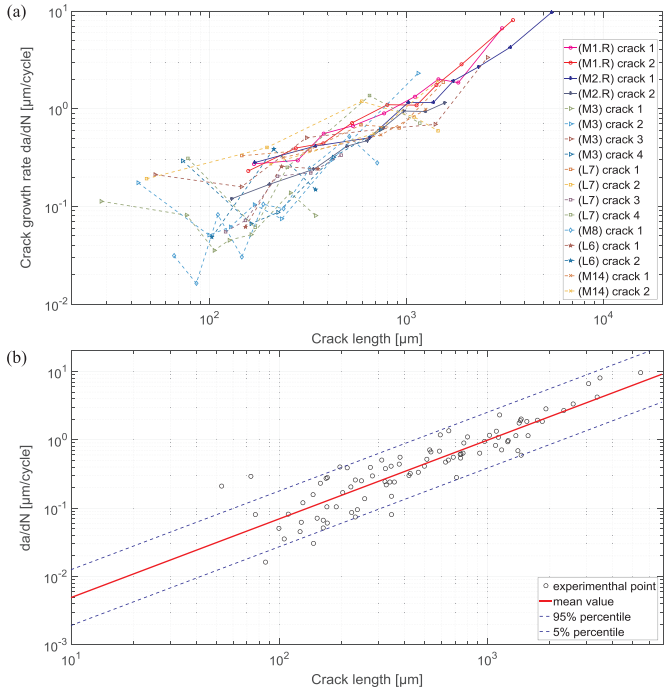

Fig. 6. Crack growth rate: (a) Experimental crack growth rate vs. crack length and (b) Model calibration.

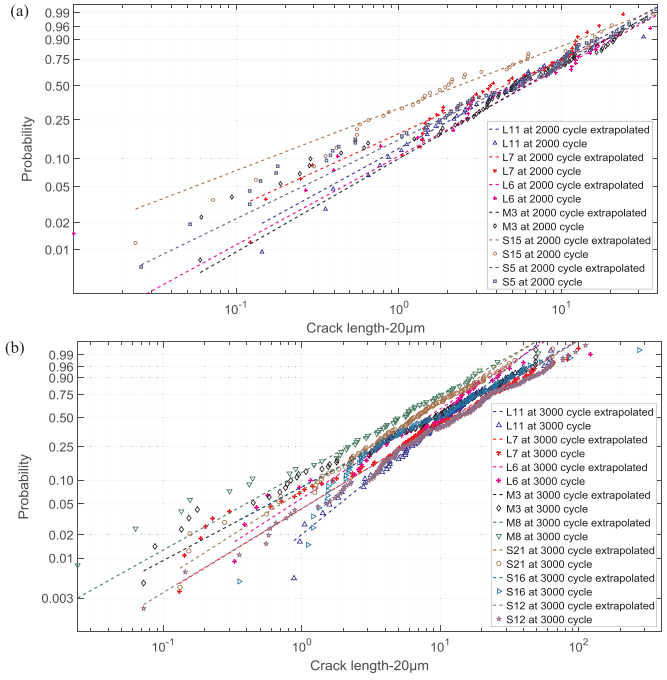

Fig. 7. Weibull distributions of surface crack length: (a) 2000 cycle and (b) 3000 cycle.

fracture morphology examples of these specimens are shown in Fig. 4.

As it can be seen from Fig. 3, similar to the reduced activation ferritic/martensitic steels [38], it's worth noting that for 30NiCrMoV12 steel, no significant specimen size effect was observed form the cyclic response curves of small, standard and large specimens, namely, the hypothesis of the size effect based on the statistical distribution of defects is not valid for this material. It should be pointed out that the four specimens (S3, S13, S14 and S22) due to original defects are not included for curve fittings in Fig. 3. From the viewpoint of tested life scatter for the three geometrical specimens, experimental lives are well described by a log-normal distribution at different loading stress levels, as shown in Table 5.

2.3.2. Crack growth rate

Note from fracture morphology inspection of fracture surfaces in Fig. 4 that multiple cracks initiated and propagated at the surface of the specimen. For the 30NiCrMoV12 steel, its fatigue life is obviously dominated by the crack propagation life rather than the crack initiation life. In order to quantify the specimen size/volume effect on fatigue life, crack growth in the presence of a marked plastic strain range within the LCF regime can be well described by using the Tomkins model [39], which has been included in the British R6 procedure as the fundamentals of short crack growth modeling. Through assuming the amount of crack growth per cycle under tension-compression loadings to be the amount of irreversible shear decohesion occurs at the crack tip, Tomkins [39] links the crack growth to the plastic strain amplitude by an exponential law

$$\begin{cases} a = a_i e^{k_g N} \\ k_g = k_{g0} \varepsilon_{pa}^{\tau} \end{cases} \quad (4)$$

Table 6
Experimental crack length and density.

Parameters		S5	S12	S15	S16	S21	M3	M8	L6	L7	L11
2000 cycle	α	4.900	–	7.860	–	–	6.958	–	8.721	6.672	6.997
	β	0.842	–	0.839	–	–	0.889	–	0.872	1.020	0.980
	λ	24.3	–	13.6	–	–	22.3	–	11.1	15.8	21.3
3000 cycle	α	–	9.006	–	12.17	19.729	11.752	8.564	12.879	17.005	14.829
	β	–	1.074	–	1.073	1.119	0.971	0.984	1.115	1.052	1.259
	λ	–	35.6	–	35.6	49.7	38.5	23.17	13.9	39.2	28.4

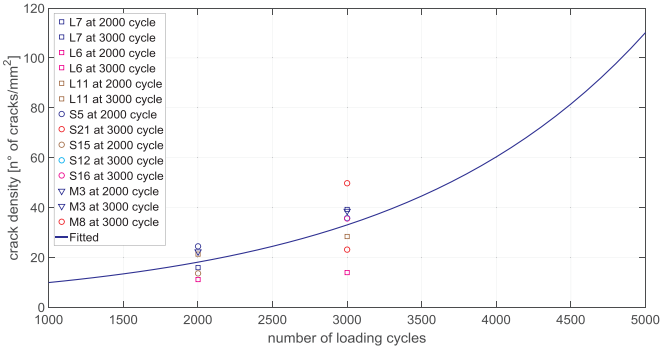

Fig. 8. Crack density varies with load life ratio.

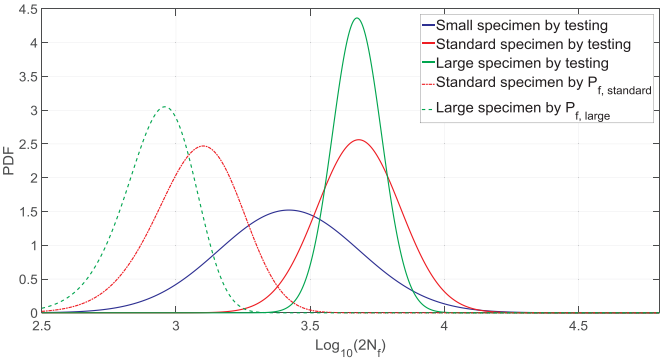

Fig. 9. Expected life based only on size effect due to statistic of extremes.

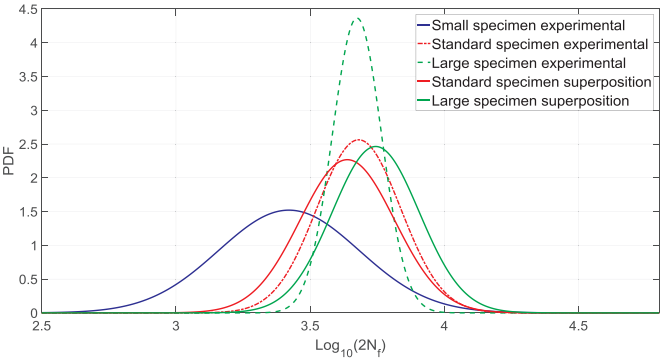

Fig. 10. Comparison between extracted distribution and experimental ones.

where a and a_i are the crack length and initial crack length, respectively; ε_{pa} is the plastic strain amplitude, k_{g0} and τ are material parameters that establish the short cracks growth in a material.

Then, crack growth rate is derived as

$$\frac{da}{dN} = k_{g0}\varepsilon_{pa}^{\tau} a \tag{5}$$

Through merging all the coefficients in the right term of Eq. (5), a simplified propagation model is expressed as

Table 7
Mean and scatter of the life cycles at $\varepsilon_a = 0.5\%$ due to the combination of propagation and statistical distribution of defects.

		Experimental $/\log_{10}(Cycle)$	Extracted $/\log_{10}(Cycle)$	$\mu\%$ error
Standard spec.	Mean	3.6807	3.6382	1.15%
	Std.	0.1557	0.1759	
Large spec.	Mean	3.6742	3.7441	1.90%
	Std.	0.0914	0.1620	

$$\frac{da}{dN} = k_g a \tag{6}$$

Using Eq. (6), two notched fatigue tests as mentioned in Section 2.2, were conducted with replicas to evaluate the fatigue crack growth behavior of 30NiCrMoV12 steel at $\varepsilon_a = 0.5\%$. Crack lengths are measured from the micro-holes of notched specimens and the gauge surface of smooth specimens. Fig. 5 shows an example crack evolution near the micro-hole of M1.R specimen. Combining with surface crack evolutions of smooth and notched specimens at different life cycles, the experimental crack growth rate can be calculated and plotted as shown in Fig. 6**(a)**, which provides a data base for fatigue crack growth model calibration (see Section 3.2). Parameters of Tomkins model are calibrated from abovementioned experiments, as shown in Fig. 6**(b)**, which reported the interpolated experimental data and the ones fitted by Eq. (6). Particularly, crack growth parameter $\log10(k_g)$ in Eq. (6) is fitted by a normal distribution from the measured surface cracking behavior, namely, $\log10(k_g) \sim N(-3.45888, 0.248095)$.

2.3.3. Surface crack density and distribution

During the replica tests, a large number of surface cracks were generated and noticed by replicas of the smooth specimen, even after a low number of loading cycles. Specifically, the specimens were tested to a given number of loading cycles, such as 2000 and 3000 loading cycles, then surface cracks were observed in a given area of 6 mm^2 at the central part of the specimen by optical micrographs. The size distribution, density and angle of these cracks were examined by the micrographs, which have shown a two-dimensional random distribution. Note from [26,39–41] that Weibull distribution can fit well the surface crack distribution. Accordingly, a three-parameter Weibull distribution is introduced in this analysis based on a threshold of minimum crack length measure, namely $a_0 = 20\mu m$. Based on the measured crack data, Weibull coefficients and its probability plot can be obtained by

$$P(a) = 1 - exp\left(-\left(\frac{a - a_0}{\alpha}\right)^{\beta}\right) \tag{7}$$

where β and α are the Weibull shape parameter and scale parameter, and a_0 is the resolution of crack identification.

Using Eq. (7), Fig. 7 plots the Weibull distributions of surface cracks measured from 10 specimens at 2000 and 3000 loading cycles, respectively. Note that these distributions shift to the right x-axis with crack propagation.

Moreover, crack density, $\lambda(No./mm^2)$, is evaluated by the ratio between the number of cracks (crack length $a \geq 20\mu m$) and the surface

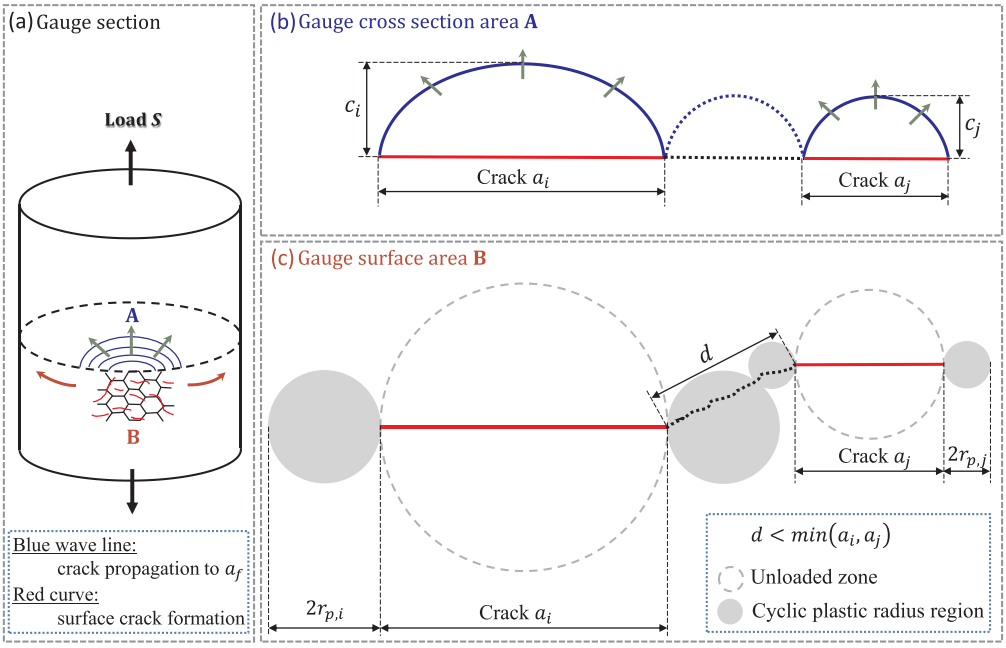

Fig. 11. Scheme of crack coalescence and influence zones.

area A. Based on this, experimental crack growth rate and density are measured during testing as shown in Table 6. Fig. 8 shows an increase of surface crack density λ with the increase of loading cycles, which is in a percentage with observations of surface cracks. According to [26], this relationship can be specifically simplified by a power law function of the load life ratio $\left(\frac{n}{N_f}\right)$

$$\lambda = C_1 exp\left(C_2 \frac{n}{N_f}\right) = f(n) \tag{8}$$

where C_1 and C_2 are fitted coefficients related to the loading conditions. Generally, the initiation density of surface cracks is affected by various factors, such as loading conditions, the number of loading cy-cles, material properties and so on. For the current tests, the crack density can be expressed by $\lambda = f(n)$. The surface crack density and distribution obtained in this section will be used as inputs for crack growth modeling and multiple surface fracture simulation in Section 4.

3. Mechanical-probabilistic modeling of size effect on total fatigue life

3.1. Prediction of specimen size effect based on the weakest-link theory

The weakest-link theory was originally presented to describe the tensile fracture of brittle materials by introducing a Weibull probability distribution of failure. Specifically, due to the randomly distributed material defects (non-homogeneities, inclusions, precipitates) in a material per volume unit, the theory states that fatigue crack initiates where the most dangerous defect or the weakest link exists [15,42,43]. Fatigue cracks propagate independently in different areas. Thus, a statistical distribution of random defects within structures/components often gives rise to the scatter in the fatigue behavior of the material. Similar to Eq. (7), through relating the effect of load and cross-sectional area or volume with the fatigue life, a classic form of the Weibull distribution for the failure probability can be expressed as

$$P_f(\sigma, \Omega) = 1 - exp\left[-\frac{1}{\Omega_0}\int^{\Omega} f(\sigma) d\Omega\right] \tag{9}$$

where Ω_0 is the reference volume or surface; $f(\sigma)$ is a function of the risk of rupture with three parameters

$$f(\sigma) = \left(\frac{\sigma - \sigma_u}{\sigma_0}\right)^m \tag{10}$$

where m and σ_0 are the shape parameter and scale parameter of the Weibull distribution, respectively; σ_u is the threshold stress, and Eq. (9) describes a two-parameter Weibull distribution when $\sigma_u = 0$.

For a given stress level, the fatigue life has shown a certain scatter in a logarithmic life scale, its cumulative distribution function (CDF) of failure probability can be expressed by a function of fatigue failure life N

$$P_f(N) = 1 - exp\left[-\left(\frac{logN}{logN_0}\right)^m\right] \tag{11}$$

where N_0 is the reference fatigue life under the given stress level.

For a metal solid consists of n elements, its survival probability can be estimated from the product of survival probabilities of each volume/surface element within the solids. Assuming that each element has volume/surface Ω_0, then $\eta = \Omega/\Omega_0$. Combining Weibull power law with Eq. (10) yields the following two-parameter Weibull distribution

$$P_f(N) = 1 - \left\{exp\left[-\left(\frac{\sigma}{\sigma_0}\right)^m\right]\right\}^{\eta} \tag{12}$$

By using Eq. (9) for describing the life (as done by Wormsen et al. [43]), the distribution of experimental results can be derived for specimens with different geometries (such as cross-sectional areas). As aforementioned, fatigue cracks initiate from the material defects. In general, an increasing of specimen/component volume or surface increases its probability of failure due to the higher probability to find a critical defect. Based on Eq. (11), a relation can be obtained for two different specimen sizes under a similar failure probability

$$\frac{N_2}{N_1} = \left(\frac{A_1}{A_2}\right)^{\frac{1}{m}} \tag{13}$$

where N_1 is the fatigue life for a specimen with the known surface or cross-sectional area A_1, N_2 is the estimated fatigue life for the specimen with determined surface or cross-sectional area A_2. In the current study, since the gauge section of the fatigue specimens yields the main and

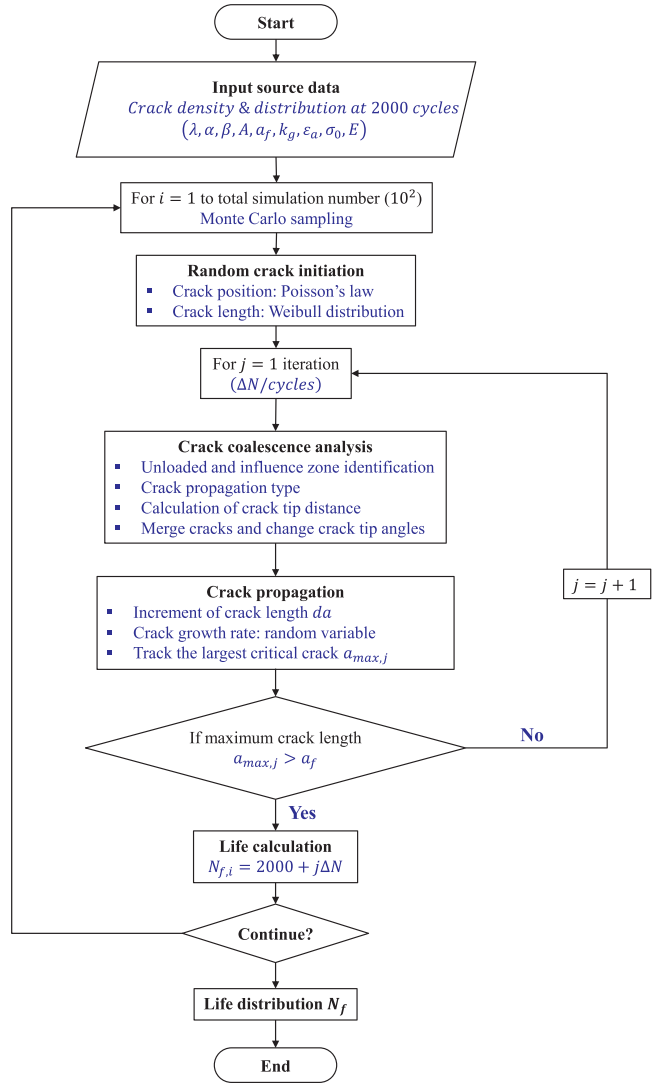

Fig. 12. Main flow chart of multiple fracture simulation.

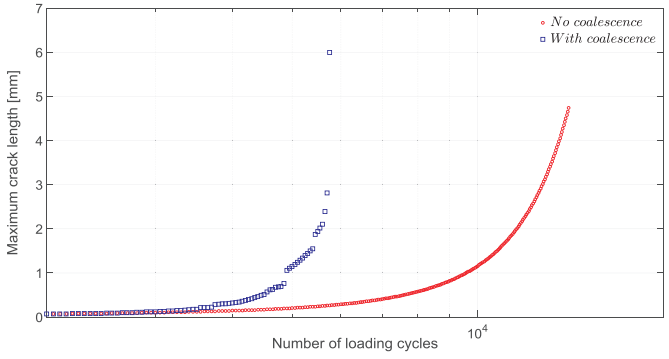

Fig. 13. Comparison between the maximum crack length with and without coalescence.

dominating contribution to the fatigue life integrals of Eq. (13), A_1 and A_2 are calculated over the gauge section of different sizes of specimens.

Similarly, adopting Eqs. (12) and (13) and taking the distribution of fatigue life of small specimens as a reference, the distribution of the life for large and standard specimens can be expressed by a function of the probability of failure of small specimens $P_{f,small}$ as

$$P_{f,standard} = 1-[1-P_{f,small}]^{\eta_{standard}} \tag{14}$$

$$P_{f,large} = 1-[1-P_{f,small}]^{\eta_{large}} \tag{15}$$

where the two coefficients $\eta_{standard}$ and η_{large} are the ratio between the gauge surfaces of the standard/large specimens and the small ones, respectively.

Under a log-normal life distribution of different sizes of specimens, Fig. 9 plots life distributions of the standard and large specimens according to Eqs. (12) and (13). Comparing with experimental mean and scatter of the life cycles at $\epsilon_a = 0.5\%$, a consequence of the distribution of defects based on statistic of extremes cannot explain well the tested life distributions as shown in Fig. 9, which coincides with the challenge raised by Todinov [43–45].

3.2. Prediction of specimen size effect based on crack propagation modeling

As aforementioned, the fracture morphology inspections of fracture surfaces have shown multiple cracks initiated and propagated at the surface of the specimen. For the specimen size effect, it normally shows a negative effect on fatigue life from the viewpoint of defects, however, a positive effect from the aspect of crack growth. Particularly, the cri-tical crack length for fatigue fracture increases with the larger specimen size/volume, especially for crack propagation process dominated ma-terials. Considering both these negative and positive effects can lead to a robust evaluation of strain-controlled fatigue behavior against spe-cimen size. Thus, the influence of specimen geometrical size on fatigue crack propagation life is critical essential for a theoretical under-standing of fatigue lives.

Through using the Tomkins model for crack growth modeling, the number of cycles to failure N_f can be estimated by integrating Eq. (6) from an initial crack length a_i to the final one a_f

$$\int_{a_i}^{af} \frac{da}{a} = \int_0^{N_f} k_g dN \Rightarrow \Delta N = \frac{1}{k_g} ln\left(\frac{\log_{10}(a_f)}{\log_{10}(a_i)}\right) \tag{16}$$

Based on the calibrated Tomkins model in Eq. (16), two scale factors can be defined to shift the distribution found with the statics of extremes for the standard and large specimens from the reference small one

$$\gamma_{standard} = \frac{\Delta N_{standard}}{\Delta N_{small}} = \frac{ln\left(\frac{\log_{10}(af,\ standard)}{\log_{10}(a_i)}\right)}{ln\left(\frac{\log_{10}(af,small)}{\log_{10}(a_i)}\right)} \tag{17}$$

and

$$\gamma_{large} = \frac{\Delta N_{large}}{\Delta N_{small}} = \frac{ln\left(\frac{\log_{10}(af,\ large)}{\log_{10}(a_i)}\right)}{ln\left(\frac{\log_{10}(af,small)}{\log_{10}(a_i)}\right)} \tag{18}$$

Combining Eq. (14) to Eq. (18), the life scale factors at $\epsilon_a = 0.5\%$ due to the propagation size effect can be calculated from $a_i = 100\mu m$ to $a_f = \frac{\pi D_0}{2}$ (according to the fracture surfaces measurement, the final crack length for all the specimens is taken half of the cross-sectional perimeter of the specimen), namely, $\gamma_{standard} = 1.18048$ and $\gamma_{large} = 1.27523$.

As pointed out by Koyama et al. [21], the specimen size effect can be quantified by the sum of the effect of statistical distribution of the defects and the effect of crack propagation. From a crack growth point of view, a larger size of specimen would lead to a longer life, which shift the dotted/dash lines in Fig. 9 to the right-hand of the x-axis. According to this, a comparison between the curves of experimental distribution of the life and the ones due to the effects of statistical defects and crack propagation can be made by using Eqs. (17) and (18), as shown in Fig. 10. Moreover, a quantitative analysis is conducted and results are listed in Table 7. As it can be seen, the influence of specimen size on fatigue life of 30NiCrMoV12 steel can be fairly predicted by summing the effects of statistical distribution of defects (negative factor) and crack propagation (positive factor).

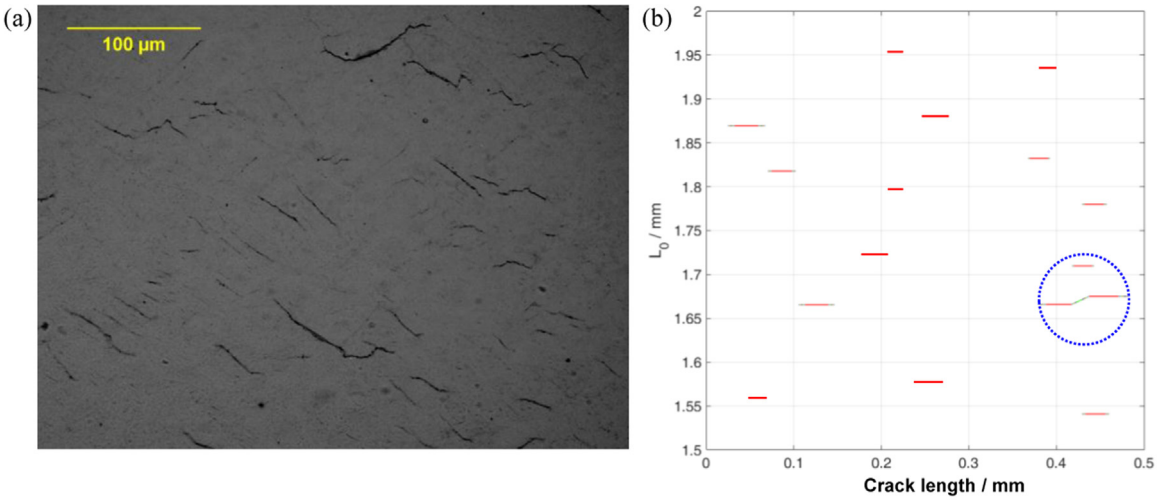

Fig. 14. Scheme of crack distribution and unloaded zones (a) experimental of S12 at 3000 cycle and (b) simulation.

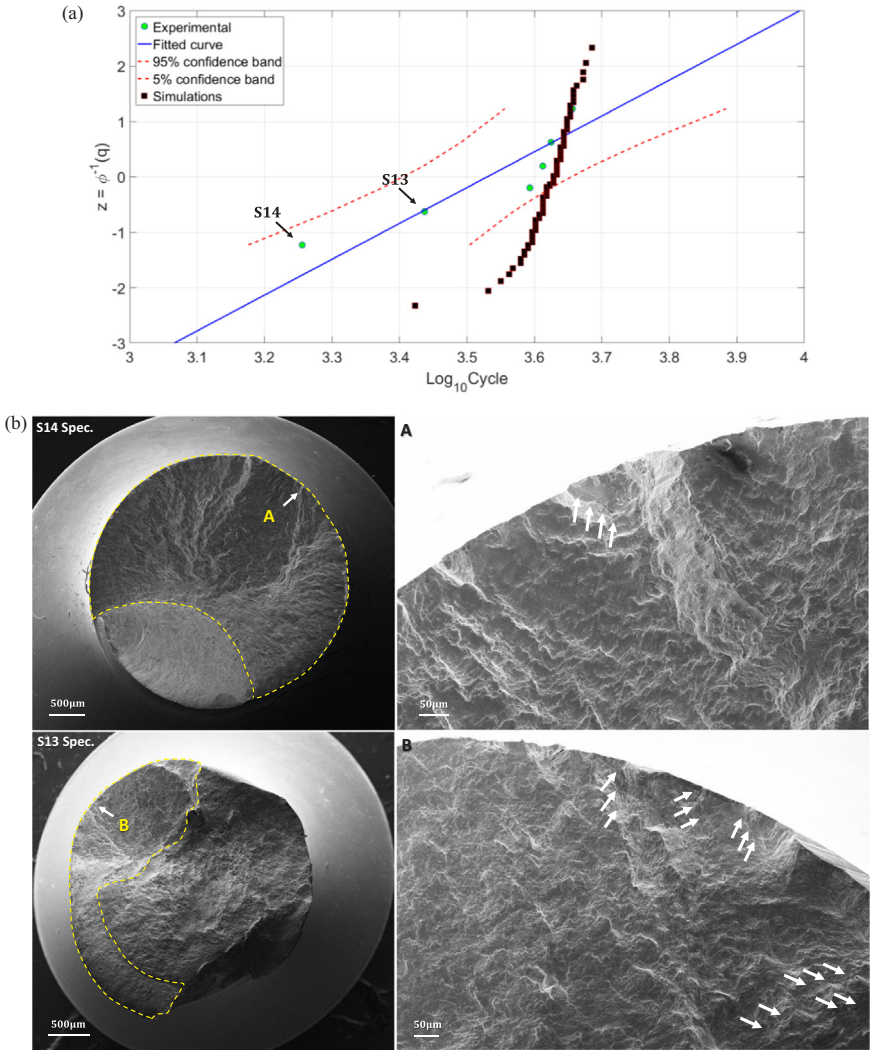

Fig. 15. Comparison between simulations and experimental lives according to small specimens: (a) probability plot and (b) fracture surfaces of S13 and S14.

4. Numerical modeling of multiple surface fracture

As aforementioned, the weakest-link theory assumed that the critical defects are sparsely distributed without interactions with each other, which only works with a low density of large metallurgical defects. However, note from Section 2.3.3 that, high density of fatigue short microcracks is observed at the gauge section surface of the specimen. The abovementioned assumption is therefore likely to be less

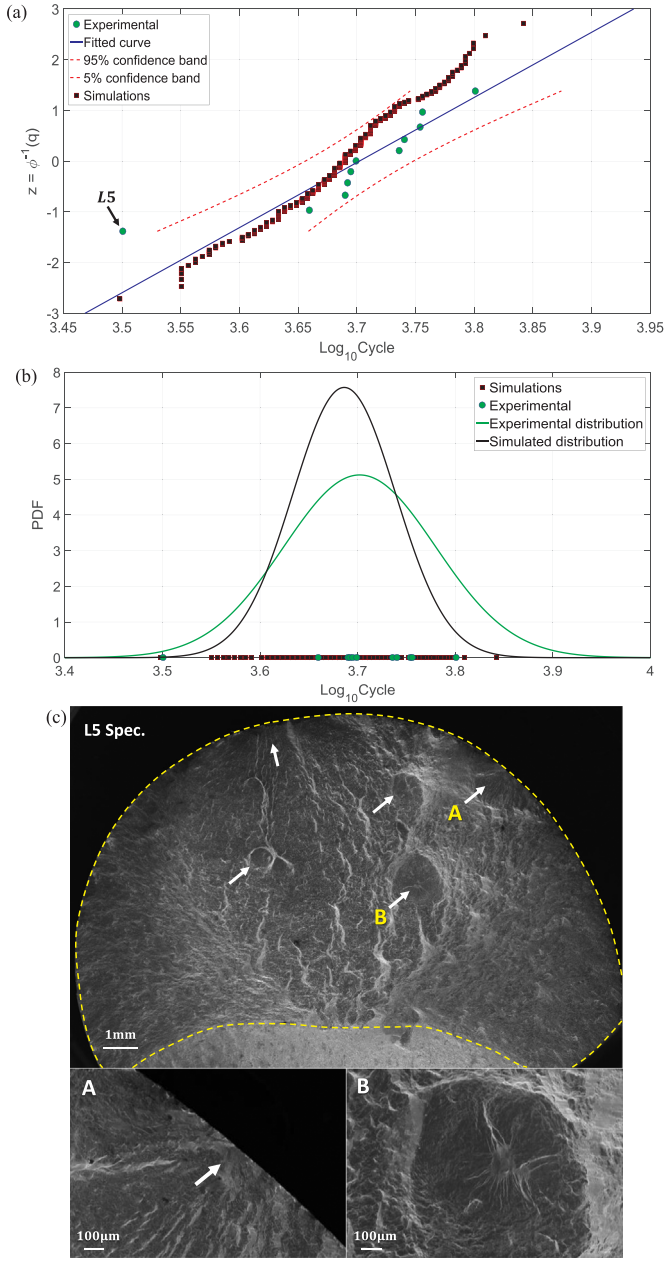

Fig. 16. Comparison between simulations and experimental lives according to large specimens: (a) probability plot, (b) life distribution and (c) fracture surfaces of L5.

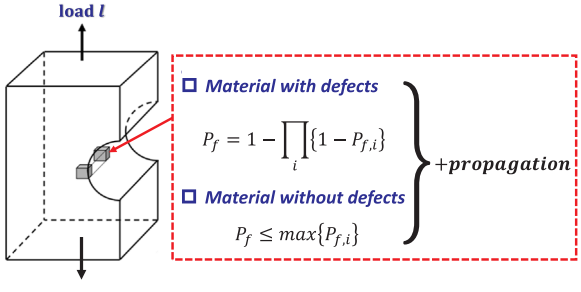

Fig. 17. Scheme of fatigue design under size/volume effects.

appropriate, especially when such surface microcracks are leading to the fatigue failure of the specimen. In this regard, further simulations with known surface crack distributions are conducted to provide a better understanding of specimen size effect.

As noticed from Fig. 4, the presence of multiple (dispersed or multisite) surface cracks scatted over the gauge section is the main manifestation of damages in 30NiCrMoV12 steel under cyclic loadings. In particular, its fracture was induced by the mutual processes of crack formation, growth and coalescence. Since surface crack sizes and locations are randomly distributed in the gauge section of the specimen, the progressive process of crack interaction and coalescence will be analyzed by combining a Monte Carlo simulation and statistical analysis of cracks. Generally, multiple surface fracture is of stochastic nature due to the random process of crack formation, as well as dis-persed crack lengths and their growth rates with potential coalescences [46–48]. According to the interaction and coalescence of short cracks, the dimension of main cracks exhibits a jump-like increase way. Specifically, an unexpected formation of a critical crack may be generated under high density of short cracks. Combining with the replica tests as mentioned in Section 2 and considering the effect of crack initiation, crack propagation and coalescence, a numerical Monte Carlo simulation is performed for multiple fracture evaluation and to compare experimental data on crack length distribution evolution, as well as the experimental life of specimens with different sizes/volumes, with the simulated ones.

4.1. Surface crack modeling and simulation algorithm

The simulation conducted in this analysis includes the mutual processes of random crack formation, propagation and coalescence of surface microcracks in the gauge section of three geometrical specimens. The available experimental data make it possible to model and simulate the multiple fracture behavior, which attempts to describe the damage evolution by characterizing the appearance of a crack from initiation to propagation under crack coalescence. According to the measured experimental data from replica tests under cyclic loadings in Section 2.3, the initial prerequisites and assumptions are taken as follows.

(1) Uniform material properties of the material are assumed over the entire damaged gauge surface, namely, the simulation surface area;
(2) Uniaxial stress state is loaded and time-independent during the crack evolution;
(3) All cracks over the gauge surface are oriented normally to the loading stress direction, like the x-axis in this analysis;
(4) A constant increment of the load cycles is assigned as the count number of iterations;
(5) The positions of all cracks on the surface are randomly distributed according to Poisson's law. Particularly, the probability that n cracks are located on the area A with the crack density λ

$$P(n) = \frac{(-\lambda A)^n}{n!} exp(-\lambda A) \tag{19}$$

(6) The initial length a of the crack is assigned by a three-parameter Weibull distribution (see Section 2.3.3);
(7) In crack propagation, the crack length increment of each crack during a given number of iterations is prescribed. In particular, the stochastic nature of fatigue crack growth rate is assigned by a normal distribution measured from replica tests (see Section 2.3.3); At the initial state, such as the specimen at 2000 cycles in the current analysis, all cracks with randomly extracted positions, crack lengths and crack growth rates are created. After this, no crack initiation, just crack propagation and coalescence will be addressed;
(8) In crack coalescence, quasi-collinear surface cracks in close proximity interact based on the influence zones at its both tips, and their propagation paths change once these influence zones of two crack tips overlap [49]. Assuming that, a direct connection is soon accomplished when the crack interaction occurs. This procedure

progresses until no crack satisfies the interaction condition. The influence zone is defined by a circle of diameter r_p according to the size of local plastic deformation zone around the crack tip [50]

$$r_p = \frac{\Delta J_{eff} \bullet E'}{2\pi\sigma_0^2} \tag{20}$$

where ΔJ_{eff} is the effective cyclic J-Integral, σ_0 is the flow stress and E' is the cyclic Young's Modulus under plane strain condition, with $E' = E/(1-\nu^2)$ and ν is the Poisson's ratio. The general formulation of the effective cyclic J-Integral ΔJ_{eff} can be obtained by

$$\Delta J_{eff} = \pi Y^2 a \left[(1-\nu^2)\frac{\Delta\sigma_{eff}^2}{E} + h(n_i)\Delta\sigma_{eff}\Delta\varepsilon_{p,eff} \right] \tag{21}$$

where $\Delta\sigma_{eff}$ and $\Delta\varepsilon_{p,eff}$ are the effective stress range and effective plastic strain range, respectively; Y is a geometric factor; n_i is the cyclic stress-strain curve exponent and $h(n_i)$ is a function that accounts for crack geometry and material elastic-plastic behavior. The criterion of Murakami [51] on judging defects interaction/ coalescence is adopted, namely, coalescence of two cracks in close proximity happens once the local influence zones (marked as the grey area in circle) at their tips touch or intersect as shown in Fig. 11, in which plots the surface crack schematic, with blue wave lines for main crack propagation to the critical length for failure a_f, and red curves for crack formation on the specimen surface, by the distance between the tips d is less than the minimum of the two crack length

$$d < min(a_{crack1}, a_{crack2}) \tag{22}$$

(9) An unloaded material zone during crack propagation and coalescence is formed around each crack, of which the shape of the zone is defined by a circle on the crack with its diameter equal to the crack length a_i, namely the blue dotted circle area as shown in Fig. 11. In these zones, the crack propagation is arrested when its tip comes into the unloading zone from the nearest crack.

Based on abovementioned starting prerequisites, a simulation flow chart is given in Fig. 12, the basic inputs obtained from experimental testing for multiple fracture simulation of different geometrical specimens include the following parameters, as listed in Table 6:

(1) Crack density on the gauge surface;
(2) Damaged surface size, namely the gauge surface $A = \pi D_0 \times L_0$;
(3) Distribution of crack length and crack growth rate on the gauge surface;
(4) Fracture and failure criterion. Fracture failure of a specimen occurs when the major crack length reaches the critical crack length a_f through the repeated processes of crack propagation and coalescence.

By using the abovementioned procedure and data, multiple surface fracture processes, in which randomly distributed cracks are initiating, coalescing and propagating to cause final fracture, can be simulated. Fig. 13 presents a comparison between the maximum crack length with and without considering coalescence of cracks, in which the process of crack coalescence has significantly shortened the lifetime during the later stage of crack propagation.

4.2. Simulation results and discussions

For this Monte Carlo-based simulation, the material damaging under cyclic loading can be characterized by crack initiation, propagation and coalescence. Note that surface cracks, a typical example of randomly distributed surface cracks of S12 at 3000 cycle, are dispersed over the surface with different lengths as shown in Fig. 14**(a)**, corresponding simulation result is given in Fig. 14**(b)**, in which circles mark the unloaded zones after the crack coalescence. The interaction and coalescence of surface cracks occurs when they are close enough to each other as described in Section 4.1. The probability of this tendency is much more frequent during the later stage of fatigue life as judged from qualitative observations. Thus, two mechanisms for crack propagation, including the crack length increment due to its own growth for those cracks without coalescence and sudden crack length increment due to the neighboring cracks coalescence through interacting by their tips, are introduced in this simulation. Accordingly, the largest crack exhibits stepwise increase due to merging with other cracks in the plastic radius. Through following the procedure in Section 4.1, an example probability plot of experimental and simulated lives according to small specimens is presented in Fig. 15**(a)**, and fracture surfaces of S13 and S14 in Fig. 15**(b)**. Moreover, using the surface crack data of small specimens as a reference, similar probability plots and life distributions for the big specimens can be derived as shown in Fig. 16, in which fracture surfaces of L5 with shorter life are given in Fig. 16**(c)**. As seen in Fig. 15**(a)**, the simulated life distribution covers well with the lives of small specimens except that of S13 and S14, in which their fracture surfaces have shown a worst condition on multiple surface crack interaction and propagation, like the peculiar cracks marked in Fig. 15**(b)**.

Form small specimens to large specimens as shown in Figs. 15 and 16, the statistical aspect of surface fatigue damage and simulated lifetime is a combined result of randomly short crack initiation, propagation and interaction. As it can be seen, the simulated life by the proposed procedure corresponds reasonably well with experimental failure life. Moreover, the proposed algorithm well accounts for the experimental scatter on the fatigue lifetime of 30NiCrMoV12 steel.

5. Discussions

5.1. Comparison with other studies

It is observed from the test results of 30NiCrMoV12 specimens that the specimen size effect on fatigue life is not evident in a LCF regime. For the three different geometrical specimens, a strain-life curve in Fig. 3**(a)** can be utilized for further design/assessment. However, fa-tigue lives of these specimens have shown a certain degree of scatter under different loading stress levels.

Through evidences by [51,52] indicate that the decrease in fatigue strength of engineering components is due to the presence of inhomogeneities result from material or manufacturing process. Particularly, the component fatigue strength is controlled by the size of maximum defect present in the more stressed material volumes. This assumption only works under consideration of no interactions of the defects, or limited number of potential critical defects, otherwise the maximum size of defect clusters has to be considered [52]. In presence of defects, the influence of specimen size effect on fatigue strength/life is noticeable [7,53–55] and it can be modelled by Weibull statistics [3,19,56,57] or by the statistics of extreme defects [58,59]. As for Ni based superalloys, the size effects evidenced [17], the material inhomogeneities triggering the fatigue failures but the strain concentrations in adjacent grains due to orientation mis-match [60]: it has been shown by Musinski et al. [61] that these microstructural features can be analyzed with the statistical models developed for inclusions and defects.

However, for the case of the quench and tempered steel in this analysis, a high density of fatigue short microcracks is observed at the gauge section surface of the specimen, as noticed from Section 2.3.3. For the influence of quenching and tempering on microstructural development of this steel, the optimized quenching and tempering process decrease the size of the PAG grains [5].

Note from Fig. 9 that, the weakest-link assumption is not appropriate, since there is no difference in the crack distributions of the three

specimen series here tested. The absence of any effect due to *'independent material volumes'* is then further emphasized by the fact that coalescence plays a significant role in determining the specimen failure. (So failure of a material volume depends on what happens in the elements next to it).

Another observation has to be made about the apparent contradiction between the present results and the ones by Blasón et al. [20]: the present three different geometrical specimens were made from the same steel bar, while perhaps the 'batch-to-batch' variability plays a role in the tests reported in [20].

5.2. Consequences for fatigue design

It is worth discussing the present results also in the light of consequences for design. Fatigue design curves according to the ASME Code Section III [62], can be obtained from the best-fit curves of experimental data by first mean stress correction and then reducing fatigue life at the design point through adjusting the curve by a factor of 2 on strain (or stress) or 20 on lifecycles, which often leads to a more conservative design. In particular, these two factors were introduced to take into account the data scatter (including material variability) and differences from surface condition and size effect between the test specimens and actual components [63]. Comments by Cooper [64] on the Section III fatigue design code indicated that the factor of 20 on life can be interpreted by the product of three subfactors, including 2 on scatter of data, 2.5 on size effect and 4 on surface condition. Among them, a factor of 2.5 on size effect was suggested to the small-specimen data for estimating life of larger-specimens or actual components.

However, this deviates from present experimental observations of 30NiCrMoV12 steel. In particular, according to Fig. 9, the 'weakest-link' life factors for small-to-standard and standard-to-large specimens are 2.1807 and 1.3996, respectively, but this effect is counteracted by the crack propagation as we discussed in Section 3. Therefore, the combination of the two effects looks to be the correct approach to mitigate the excessive conservatism of the weakest-link approach even in the presence of materials with defects.

The same effect can be better explained in probabilistic concepts. Let us suppose that for a notched component modelled with finite elements, the cyclic response for the *ith* element with a volume V_i is known (for the sake of simplicity we refer to the element centroid, for a more refined approach see [17–19]). The nucleation life, in terms of nucleation of crack life with the same size of a finite element, could be at a given number of cycles estimated by a suitable model (like the Fatemi-Socie parameter $\gamma_{a,eq}$ [14]). Considering the resistance of the *ith* element (expressed in terms of life distribution $F_{\mathfrak{R}}$ at a given $\gamma_{a,eq}$), it lies within the bounds:

$$1-(1-F_{\mathfrak{R}}(\gamma_{a,eq}))^{V_i/V_0} \le F_{\mathfrak{R}}(\gamma_{a,eq,i}) \le F_{\mathfrak{R}}(\gamma_{a,eq}) \tag{23}$$

where V_i is the element volume and V_0 is the reference material volume (onto which the tests were carried out). The left term corresponds to 'independent material volumes' (according to the weakest-link concept), while the right one corresponds to perfectly correlated material volumes.

As a consequence of Eq. (23), the failure probability P_f for the component is

$$1-\prod(1-P_{f,i}) \le P_f \le max P_{f,i} \tag{24}$$

According to the present findings, the right term of Eq. (24) is the correct approach when there are no defects (or microstructural inhomogeneities) in the material that could support the choice of the 'weakest-link' model (see Fig. 17). The fatigue life (or its distribution) could then be estimated by adding to the nucleation time (life to failure of the most stressed element) and the propagation lifetime. An alternative to crack propagation algorithms such as Darwin [65], would be to simply adopt a multiplication factor (based on a suitable propagation model) such as Eqs. (17) and (18).

6. Conclusions

In the present study, to explain the robustness against specimen size, normal strain-controlled fatigue and replica tests with three geometrical specimens are carried out for evaluating the influence of specimen size on fatigue life of 30NiCrMoV12 steel in a LCF regime. The main results are summarized as follows:

(1) Experimental results and fractographic analyses show that its fatigue life is mainly dominated by the crack propagation life rather than the crack initiation life, which consists of multiple surface cracking with mutual interactions and coalescences.
(2) No significant differences in the life of different material volumes were observed because of the absence of independent features (defects and/or microstructural inhomogeneities) that able to trigger the failure;
(3) A probabilistic procedure for multiple surface fracture simulation is established by incorporating random processes of crack formation, propagation and coalescence between dispersed surface cracks, which elaborates an evaluation of statistical surface damage evolution for different structural sizes/volumes and supports the experimental findings;
(4) The 'weakest link' (shorter lifetime for larger material volumes) effect is counteracted by the propagation lifetime (larger propagation time for larger volumes): an approach based on the two effects seems to be the most appropriate and even able to better describe the present findings.

Acknowledgments

Dr. S.P. Zhu acknowledges support for his period of study at Politecnico di Milano by the Polimi International Fellowship Grant scheme. The authors acknowledged support by Lucchini RS (Italy) for supplying the heat treated steel. The authors also wish to thank Mr. Carlo Marzorati, who was a previous student of Politecnico di Milano, for taking care of fatigue and crack growth experiments.

References

[1] M.J. Alava, P.K.V.V. Nukala, S. Zapperi, Size effects in statistical fracture, J. Phys. D Appl. Phys. 42 (21) (2009) 214012.
[2] Y. Murakami, Material defects as the basis of fatigue design, Int. J. Fatigue 41 (2012) 2–10.
[3] P.C. Gope, Determination of sample size for estimation of fatigue life by using Weibull or log-normal distribution, Int. J. Fatigue 21 (1999) 745–752.
[4] K.H. Kloos, A. Buch, D. Zankov, Pure geometrical size effect in fatigue tests with constant stress amplitude and in programme tests, Materwiss. Werksttech. 12 (1981) 40–50.
[5] Y. Zheng, F. Wang, C. Li, Y. Li, J. Cheng, R. Cao, Effect of microstructure and precipitates on mechanical properties of Cr-Mo-V alloy steel with different austenitizing temperatures, ISIJ Int. 58 (6) (2018) 1126–1135.
[6] S. Beretta, A. Ghidini, F. Lombardo, Fracture mechanics and scale effects in the fatigue of railway axles, Eng. Fract. Mech. 72 (2005) 195–208.
[7] S.C. Wu, S.Q. Zhang, Z.W. Xu, G.Z. Kang, L.X. Cai, Cyclic plastic strain based damage tolerance for railway axles in China, Int. J. Fatigue 93 (2016) 64–70.
[8] M. Shirani, G. Härkegård, Fatigue life distribution and size effect in ductile cast iron for wind turbine components, Eng. Fail. Anal. 18 (2011) 12–24.
[9] L. Makkonen, R. Rabb, M. Tikanmäki, Size effect in fatigue based on the extreme value distribution of defects, Mater. Sci. Eng. A 594 (2014) 68–71.
[10] M. Makkonen, Statistical size effect in the fatigue limit of steel, Int. J. Fatigue 23 (5) (2001) 395–402.
[11] A. Carpinteri, A. Spagnoli, S. Vantadori, Size effect in S-N curves: a fractal approach to finite-life fatigue strength, Int. J. Fatigue 31 (5) (2009) 927–933.
[12] S. Beretta, S. Romano, A comparison of fatigue strength sensitivity to defects for materials manufactured by AM or traditional processes, Int. J. Fatigue 94 (2017) 178–191.
[13] O. Hertel, M. Vormwald, Statistical and geometrical size effects in notched members based on weakest-link and short-crack modelling, Eng. Fract. Mech. 95 (2012) 72–83.
[14] S. Zhu, S. Foletti, S. Beretta, Probabilistic framework for multiaxial LCF assessment under material variability, Int. J. Fatigue 103 (2017) 371–385.

[15] T. Tomaszewski, J. Sempruch, T. Piatkowski, Verification of selected models of the size effect based on high-cycle fatigue testing on mini specimens made of EN AW-6063 Aluminum alloy, J. Theor. Appl. Mech. 52 (4) (2014) 883–894.

[16] R. Wang, D. Li, D. Hu, F. Meng, H. Liu, Q. Ma, A combined critical distance and highly-stressed-volume model to evaluate the statistical size effect of the stress concentrator on low cycle fatigue of TA19 plate, Int. J. Fatigue 95 (2017) 8–17.

[17] S. Schmitz, T. Seibel, T. Beck, G. Rollmann, R. Krause, H. Gottschalk, A probabilistic model for LCF, Comput. Mater. Sci. 79 (2013) 584–590.

[18] L. Made, H. Gottschalk, S. Schmitz, T. Beck, G. Rollmann, Probabilistic LCF risk evaluation of a turbine vane by combined size effect and notch support modeling, in: Proceedings ASME Turbo Expo 2017 Turbomach. Tech. Conference Expo. Charlotte, North Carolina, USA, June 26–30, 2017.

[19] L. Made, S. Schmitz, H. Gottschalk, T. Beck, Combined notch and size effect modeling in a local probabilistic approach for LCF, Comput. Mater. Sci. 142 (2018) 377–388.

[20] S. Blasón, M. Muniz-calvente, R. Koller, C. Przybilla, A. Fernández-canteli, Probabilistic assessment of fatigue data from shape homologous but different scale specimens. Application to an experimental program, Eng. Fract. Mech. 185 (2017) 193–209.

[21] M. Koyama, H. Li, Y. Hamano, T. Sawaguchi, Mechanical-probabilistic evaluation of size effect of fatigue life using data obtained from single smooth specimen: an example using Fe-30Mn-4Si-2Al seismic damper alloy, Eng. Fail. Anal. 72 (2017) 34–47.

[22] Y. Murakami, K.J. Miller, What is fatigue damage ? A view point from the observation of low cycle fatigue process, Int. J. Fatigue 27 (2005) 991–1005.

[23] J. Stolarz, Multicracking in low cycle fatigue-a surface phenomenon? Mater. Sci. Eng. A 234–236 (1997) 861–864.

[24] B. Fedelich, A stochastic theory for the problem of multiple surface crack coalescence, Int. J. Fract. 91 (1998) 23–45.

[25] S. Beretta, P. Clerici, Microcrack propagation and microstructural parameters of fatigue damage, Fatigue Fract. Eng. Mater. Struct. 19 (9) (1996) 1107–1115.

[26] C.M. Suh, J.J. Lee, Y.G. Kang, H.J. Ahn, B.C. Woo, A simulation of the fatigue crack process in type 304 stainless steel at 538 °C, Fatigue Fract. Eng. Mater. Struct. 15 (7) (1992) 671–684.

[27] M. Liao, Probabilistic modeling of fatigue related microstructural parameters in aluminum alloys, Eng. Fract. Mech. 76 (5) (2009) 668–680.

[28] M. Liao, G. Renaud, N. Bellinger, Probabilistic modeling of short-crack growth in airframe aluminum alloys, J. Aircr. 45 (4) (2008) 1105–1111.

[29] T. Hoshide, Biaxial fatigue life predicted by crack growth analysis in various material microstructures modeled by Voronoi-Polygons, J. Mater. Eng. Perform. 20 (9) (2011) 1497–1504.

[30] M. Besel, A. Brueckner-Foit, Surface damage evolution of engineering steel, Fatigue Fract. Eng. Mater. Struct. 31 (10) (2008) 885–891.

[31] M. Besel, A. Brueckner-Foit, F. Zeismann, A. Gruening, J. Mannel, Damage accumulation of graded steel, Eng. Fail. Anal. 17 (3) (2010) 633–640.

[32] T. Hoshide, K. Kusuura, Life prediction by simulation of crack growth in notched components with different microstructures and under multiaxial fatigue, Fatigue Fract. Eng. Mater. Struct. 21 (1998) 201–213.

[33] ASTM Standard E606. Standard practice for strain-controlled fatigue testing, in: ASTM International West Conshohocken, PA, 2012.

[34] ASTM Standard E739. Standard practice for statistical analysis of linear or linearized stress-life (S-N) and strain-life (ε-N) fatigue data, in: ASTM International West Conshohocken, PA, 2015.

[35] T.S. Hahn, A.R. Marder, Effect of electropolishing variables on the current density-voltage relationship, Metallography 21 (1988) 365–375.

[36] UNI 6787-71, Assi fucinati di acciaio speciale legato, bonificati, ad elevate caratteristiche di fatica e di tenacità per sale montate di rotabili ferroviari. Qualità, prescrizioni e prove, Ente Nazionale Italiano di Unificazione, 1971.

[37] F. Corea, Modelli e prove di propagazione a fatica a basso numero di cicli in stato di sforzo multiassiale, Politec. di Milano, Master Thesis, 2011.

[38] T. Hirose, H. Sakasegawa, A. Kohyama, Y. Katoh, H. Tanigawa, Effect of specimen size on fatigue properties of reduced activation ferritic/martensitic steels, J. Nucl. Mater. 283–287 (2000) 1018–1022.

[39] B. Tomkins, Fatigue crack propagation - an analysis, Philos. Mag. 18 (155) (1968) 1041–1066.

[40] M. Goto, Y. Yanagawa, H. Nisitani, Statistical property in the initiation and propagation of microcracks of a heat-treated 0.45% C steel, JSME Int. J. Ser. 1 Solid Mech. Strength Mater. 33 (2) (1990) 235–242.

[41] M. Goto, Statistical investigation of the behavior of microcracks in carbon steels, Fatigue Fract. Eng. Mater. Struct. 14 (8) (1991) 833–845.

[42] F.W. Zok, On weakest link theory and Weibull statistics, J. Am. Ceram. Soc. 100 (2017) 1265–1268.

[43] A. Wormsen, B. Sjödin, G. Härkegård, A. Fjeldstad, Non-local stress approach for fatigue assessment based on weakest-link theory and statistics of extremes, Fatigue Fract. Eng. Mater. Struct. 30 (12) (2007) 1214–1227.

[44] M.T. Todinov, Is Weibull distribution the correct model for predicting probability of failure initiated by non-interacting flaws? Int. J. Solids Struct. 46 (3–4) (2009) 887–901.

[45] M.T. Todinov, The cumulative stress hazard density as an alternative to the Weibull model, Int. J. Solids Struct. 47 (24) (2010) 3286–3296.

[46] L. Ma, X. Wang, X.-Q. Feng, S.-W. Yu, Numerical analysis of interaction and coalescence of numerous microcracks, Eng. Fract. Mech. 72 (2005) 1841–1865.

[47] A. Bataille, T. Magnin, Surface damage accumulation in low-cycle fatigue: physical analysis and numerical modeling, Acta Metall. Mater. 42 (11) (1994) 3817–3825.

[48] M. Kamaya, Growth evaluation of multiple interacting surface cracks. Part II: growth evaluation of parallel cracks, Eng. Fract. Mech. 75 (2008) 1350–1366.

[49] H.Y. Yoon, S.C. Lee, Probabilistic distribution of fatigue crack growth life considering effect of crack coalescence, JSME Int. J. Ser. A Solid Mech. Mater. Eng. 46 (4) (2003) 607–612.

[50] S. Rabbolini, S. Beretta, S. Foletti, M.E. Cristea, Crack closure effects during low cycle fatigue propagation in line pipe steel: an analysis with digital image correlation, Eng. Fract. Mech. 148 (2015) 441–456.

[51] Y. Murakami, Metal Fatigue: Effects of Small Defects and Nonmetallic Inclusions, Elsevier, 2002.

[52] Y. Murakami, M. Endo, Effects of defects, inclusions and inhomogeneities on fatigue strength, Int. J. Fatigue 16 (3) (1994) 163–182.

[53] H. Bomas, M. Schleicher, Application of the weakest-link concept to the endurance limit of notched and multiaxially loaded specimens of carburized steel 16MnCrS5, Fatigue Fract. Eng. Mater. Struct. 28 (11) (2005) 983–995.

[54] G. Schweiger, K. Heckel, Size effect in randomly loaded specimens, Int. J. Fatigue 8 (4) (1986) 231–234.

[55] M. Kaffenberger, M. Vormwald, Considering size effects in the notch stress concept for fatigue assessment of welded joints, Comput. Mater. Sci. 64 (2012) 71–78.

[56] K. Wallin, Statistical aspects of fatigue life and endurance limit, Fatigue Fract. Eng. Mater. Struct. 33 (6) (2010) 333–344.

[57] M.T. Todinov, Equations and a fast algorithm for determining the probability of failure initiated by flaws, Int. J. Solids Struct. 43 (2006) 5182–5195.

[58] Y. Murakami, S. Beretta, Small defects and inhomogeneities in fatigue strength: experiments, models and statistical implications, Extremes 2 (2) (1999) 123–147.

[59] S. Romano, A. Brandão, J. Gumpinger, M. Gschweitl, S. Beretta, Qualification of AM parts: extreme value statistics applied to tomographic measurements, Mater. Des. 131 (2017) 32–48.

[60] L. Patriarca, S. Beretta, S. Foletti, S. Monti, E. Vacchieri, Crack propagation under LCF for a coarse-grained Ni-based superalloy at high temperatures, Proceedings of the Eighth International Conference Low Cycle Fatigue, Dresden, Ger., 2017, pp. 17–22.

[61] W.D. Musinski, D.L. McDowell, Microstructure-sensitive probabilistic modeling of HCF crack initiation and early crack growth in Ni-base superalloy IN100 notched components, Int. J. Fatigue 37 (2012) 41–53.

[62] W.J. O'Donnell, Code design and evaluation for cyclic loading – sections III and VIII, Rao K, Ed. Companion Guid. to ASME Boil. Press. Vessel code, vol. 2, 3rd ed., ASME, New York, 2009.

[63] S.O. Chopra; W, Review of the margins for ASME code fatigue design curve – effects of surface roughness and material variability. Tech Rep NUREG/ CR6815, ANL-02/ 39. U.S. Nuclear Regulatory Commission, Tech Rep NUREG/ CR6815, ANL-02/39. U.S. Nucl. Regul. Comm.,, 2003.

[64] W.E. Cooper, The initial scope and intent of the section III fatigue design procedure, in: Weld. Res. Counc. Inc., Tech. Inf. from Work. Cycl. Life Environ. Eff. Nucl. Appl. Clear. Florida, January 20–21, 1992.

[65] R. McClung, M. Enright, H. Millwater, G. Leverant, S. Hudak, A software framework for probabilistic fatigue life assessment of gas turbine engine rotors, J. ASTM Int. 1 (8) (2004) 1–16.